

Article

Photophysical Properties and Electronic Structure of Symmetrical Curcumin Analogues and Their BF₂ Complexes, Including a Phenothiazine Substituted Derivative

Emese Gál  and Levente Csaba Nagy * 

Department of Chemistry and Chemical Engineering, Faculty of Chemistry and Chemical Engineering, Babes-Bolyai University, Arany János Street 11, RO-400028 Cluj-Napoca, Romania; emese.gal@ubbcluj.ro

* Correspondence: levente.nagy@ubbcluj.ro

Abstract: Symmetrically substituted curcumin analogue compounds possess electron donor moieties at both ends of the conjugated systems; their difluoroboron complexes were synthesized, and their structures were fully characterized. A novel compound with enhanced photophysical properties bearing phenothiazine moieties is reported. The introduction of BF₂ into the molecular structures resulted in bathochromic shifts both in the absorption and emission spectra, indicating that the π -conjugation was more extended than the one in the initial compounds. The solvatochromic effects were studied, which in case of the phenothiazinyl-curcumin BF₂ complex was the most notable. Theoretical study of the investigated compounds was carried out using DFT and TD-DFT methods to evaluate the ground state geometries and vertical excitation energies.

Keywords: BF₂-curcumin; phenothiazine; solvatochromism; DFT/TD-DFT; fluorescence



Citation: Gál, E.; Nagy, L.C. Photophysical Properties and Electronic Structure of Symmetrical Curcumin Analogues and Their BF₂ Complexes, Including a Phenothiazine Substituted Derivative. *Symmetry* **2021**, *13*, 2299. <https://doi.org/10.3390/sym13122299>

Academic Editor: Alejandro Díaz-Moscoso

Received: 30 September 2021
Accepted: 24 November 2021
Published: 2 December 2021

Publisher's Note: MDPI stays neutral with regard to jurisdictional claims in published maps and institutional affiliations.



Copyright: © 2021 by the authors. Licensee MDPI, Basel, Switzerland. This article is an open access article distributed under the terms and conditions of the Creative Commons Attribution (CC BY) license (<https://creativecommons.org/licenses/by/4.0/>).

1. Introduction

Starting from the second half of the 20th century, organic electronics have made a significant contribution to the technological advancement of humanity. Organic electronic applications include field effect transistors, based on organic materials (OFETs), organic solar cells (OSCs), and the increasingly popular displays based on organic light-emitting diodes (OLEDs). A considerable amount of scientific effort has been invested into the study of organic fluorescent dyes, which have been found potentially applicable as the organic emitting layer in OLEDs, especially the ones that do not require a dopant in order to function properly [1]. A widely studied member of the aforementioned group of organic fluorescent dyes is the naturally occurring curcumin, and its synthetic derivatives. In its natural form, curcumin is known to present a wide range of benefits to human health, having radical scavenging, anti-inflammatory, antioxidant, antibacterial, antifungal, and antiviral activities [2], and HIV inhibition effects [3]. A very important property of the β -diketone group is the ability to form chelates with different metals and metalloids, for example with boron. Curcumin (Figure 1a) and its derivatives, among them the stable tetracoordinated organoboron complexes, have received much attention for their excellent photophysical properties [4–6].

The incorporation of BF₂ into the curcumin chromophores increases the rigidity of the 1,3-diketone unit, resulting in enhanced stability and a bathochromic shift in the absorption and emission spectra and unique near infrared (NIR) emission in solution and in solid state. As a result of these properties, these compounds are attractive for any application requiring highly absorbing and emitting materials, such as optoelectronic devices [7] and bio medicinal applications [8–10].

It is well known that phenothiazine presents an excellent electron donating ability, as it contains electron-rich nitrogen and sulfur heteroatoms in the central ring (Figure 1b). From a structural point of view, phenothiazine exhibits a rigid structure with a large π -conjugated

system and a non-planar butterfly conformation that can hinder the molecular aggregation and the formation of molecular excimers, which is favorable for achieving high photovoltage [11]. These advantages make the phenothiazine derivatives potential candidates for designing materials for organic electronic applications [12]. The main motivation for considering the incorporation of phenothiazine groups as terminal electron donor substituents was that functionalization of the phenothiazine backbone in multiple positions further allows the tuning of the photophysical properties of the molecule. Furthermore, the non-planar conformation of phenothiazine impedes the molecular aggregation in solutions and also in the solid state [13].

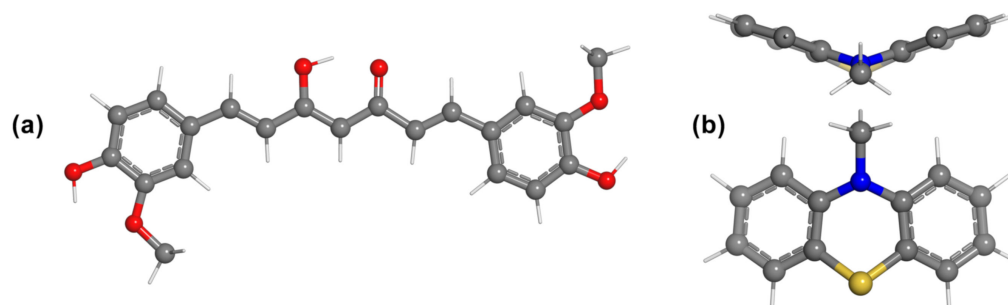


Figure 1. (a) The enol tautomer of curcumin C1; (b) the butterfly conformation of phenothiazine.

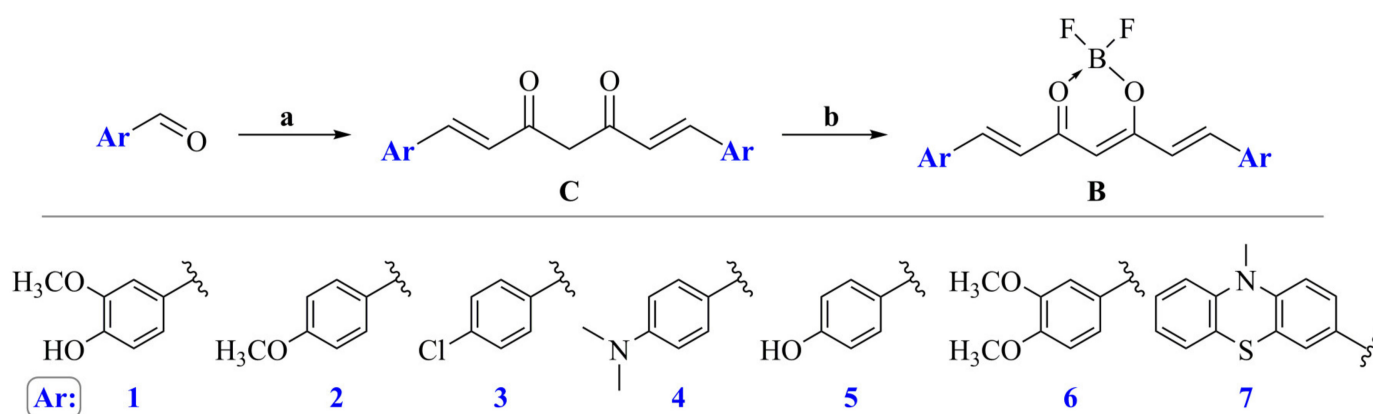
A range of studies of these BF_2 curcuminoid complexes has been reported; however, phenothiazine derivatives and the BF_2 complex have not yet been investigated as terminal aromatic moieties. The present paper is concerned with the synthesis, structural and photophysical characterization, and computational study using density functional theory (DFT) and time-dependent density functional theory (TD-DFT) of symmetric curcuminoids and their BF_2 complexes with different terminal aromatic groups, including a novel phenothiazine derivative.

2. Materials and Methods

Despite the widespread application for boron complexes of curcumin and curcumin analogs, the synthetic procedure for these compounds has remained relatively limited. The basic curcuminoid structure is formed by a simple aldol condensation reaction, the Knoevenagel condensation, catalyzed by a base between one (for symmetric product) or two different (for asymmetric product) aldehydes and 2,4-pentanedione (acetyl acetone). The advantage in the case of synthesis of symmetrically substituted curcumin derivatives is that the quantity of side products is lower, since the starting material, the aromatic aldehyde, is only one kind. In the case of heteroaromatic aldehydes as starting materials, the purification process involved the use of multiple column chromatography. In order to prevent the condensation taking place in the *meso* position, it is necessary for the β -diketone group to be held in the enol form. There are multiple ways to achieve this. The first method was described by Lampe and co-workers in 1913 [14]. A modified procedure was published by Pavolini in middle of the 20th century, who used boron trioxide; however, a very low 10% yield was obtained [15]. Later, Pabon improved Pavolini's method by adding a boric acid ester, for example tri-*n*-butyl borate, which acts as a water scavenger to prevent the decomposition of the complex [16]. As a catalyst, *n*-butylamine was used; however, the use of several other bases, such as piperidine, have been reported since then [17]. In case of vanillin and similar aldehydes, this method works well; however, the yields decrease significantly when utilizing other aldehydes, furthermore several extraction and purification steps are necessary to achieve the final product. A more recent synthetic approach was suggested by Rao et al. utilizing boron trifluoride instead of boron trioxide as a complexing agent, obtaining the BF_2 complex of the desired curcuminoid in a much higher yield. For the synthesis of the BF_2 complexes another method was also developed by Rao et al. by simply reacting the pre-existing curcuminoid with boron trifluoride etherate

in order to produce its BF_2 complex; however, the reaction time is considerably longer, and the reaction requires significantly more workup [18,19].

The syntheses of curcuminoids **C1–C6** have been reported in the literature [20,21]; in our case, we used Pabon's method with slight modifications to obtain these derivatives (**C1–C7**). As a base catalyst, instead of *n*-butylamine, isopropylamine was used, and tri-isopropyl borate served as a water scavenger. Regarding the synthesis of BF_2 complexes **B1–B7**, these were obtained by the addition of boron trifluoride etherate to the solution of the appropriate curcuminoid in diethyl ether and in the presence of acetic anhydride. The mixtures were kept at below temperatures of 0°C for 24 h. Using the acetic acid, the keto-enol equilibrium can be influenced in a way that promotes the production of the complexes. The precipitated products were then filtered, followed by multiple recrystallization steps from an acetone-water solution until the pure products were achieved (Scheme 1). The synthesized curcumin derivatives were designed to evaluate the effect by the incorporation of different electron donor moieties on the unsaturated seven-carbon spacer.



Scheme 1. Synthesis of curcumin analogues and the corresponding BF_2 complexes: (a) 2 equiv. aromatic aldehyde, acetylacetone, B_2O_3 , *i*-PrNH₂, $\text{B}(\text{O}i\text{-Pr})_3$, EtOAc, (**C1–C7**); (b) $\text{BF}_3 \cdot \text{Et}_2\text{O}$, $(\text{CH}_3\text{CO})_2\text{O}$, Et_2O , -5°C , 24 h (**B1–B7**).

All solvents used for the syntheses were of an analytic grade. Acetylacetone, vanillin, 4-methoxybenzaldehyde, 4-chlorobenzaldehyde, 4-dimethylamino-benzaldehyde, 4-hydroxybenzaldehyde, 3,4-dimethoxybenzaldehyde, boron trioxide, tri-isopropyl borate, and isopropylamine were purchased from Sigma-Aldrich. All reactions were monitored by TLC (0.25mm silica gel plates with UV indicator 60F-254, from Merck). NMR spectra (^1H , ^{13}C , and ^{19}F) were recorded at room temperature on a Bruker Avance 400 MHz spectrometer. Chemical shifts (δ) are given in ppm relative to deuterated acetone (*d*6-acetone). High-resolution mass spectra (HRMS) were obtained using Thermo LTQ Orbitrap XL (ESI+). UV-Vis absorption spectra measurements were carried out on a Perkin Elmer Lambda 35 spectrophotometer. The emission spectra were recorded using a Perkin Elmer LS 55 spectrofluorimeter.

2.1. General Procedure for the Synthesis of Curcumin Derivatives (**C1–C7**)

In a 100 mL round-bottom flask acetylacetone (8 molar equiv.), boron trioxide (7.2 molar equiv.) and ethyl acetate (5 molar equiv.) were stirred for 30 min, while being heated on a water bath and refluxed. A solution of the appropriate benzaldehyde (3.6 molar equiv.), ethyl acetate, and tri-isopropyl borate (3.6 molar equiv.) was added to the reaction mixture, and the heating was continued for another 30 min. This was followed by the addition of isopropylamine (3.6 molar equiv.) to the mixture. After 1 h, the mixture was cooled down, 10 mL 1M HCl solution was added, and stirred for 1 h. The mixture was extracted with ethyl acetate, the organic phase was dried using Na_2SO_4 , and the solvent was evaporated in a rotary evaporator. The crude product was purified using column chromatography to obtain the curcumin derivatives (**C1–C7**) in 27–80% yields.

(1E,6E)-1,7-bis(4-hydroxy-3-methoxyphenyl)-1,6-heptadiene-3,5-dione (**C1**). Orange-yellow solid, mp. 183 °C (lit. [21] 182–183 °C). The reaction yield was 58%.

(1E,6E)-1,7-bis(4-methoxyphenyl)-1,6-heptadiene-3,5-dione (**C2**). Yellow solid, mp 156 °C (lit. [21] 154–156 °C). The reaction yield was 54%.

(1E,6E)-1,7-bis(4-chlorophenyl)-1,6-heptadiene-3,5-dione (**C3**). Yellow solid, mp. 198–200 °C (lit. [20] 195–196 °C). The reaction yield was 27%.

(1E,6E)-1,7-bis(4-(dimethylamino)phenyl)-1,6-heptadiene-3,5-dione (**C4**). Purple solid mp. 213 °C (lit. [21] 206 °C). The reaction yield was 45%.

(1E,6E)-1,7-bis(4-hydroxyphenyl)-1,6-heptadiene-3,5-dione (**C5**). Dark red-orange solid mp. 222 °C (lit. [21] 226–228 °C). The reaction yield was 30%.

(1E,6E)-1,7-bis(3,4-dimethoxyphenyl)-1,6-heptadiene-3,5-dione (**C6**). Bright orange solid mp. 122 °C (lit. [21] 129–131 °C). The reaction yield was 48%.

(1E,6E)-1,7-bis(10-methyl-phenothiazinyl)-1,6-heptadiene-3,5-dione (**C7**). The compound was synthesized using 0.87 g of 3-formyl-10H-methyl-phenothiazine. ¹H-NMR (*d6*-acetone, 400 MHz), δ = 3.39 ppm (s, 6H), 5.75 ppm (s, 1H), 6.47 ppm (d, *J* = 15.76 Hz, 2H), 6.77 ppm (d, *J* = 8.56 Hz, 2H), 6.82 ppm (d, *J* = 7.64 Hz, 2H), 6.96 ppm (d, *J* = 7.48 Hz, 2H) 7.13–7.2 ppm (m, 4H), 7.31 ppm (s, 2H), 7.33 ppm (s, 2H), 7.53 ppm (d, *J* = 15.68 Hz, 2H); ¹³C-NMR (*d6*-acetone, 125 MHz), δ = 35.7 ppm; 101.9 ppm; 114.2 ppm; 114.5 ppm; 122.2 ppm; 123.1 ppm; 126.1 ppm; 127.4 ppm; 127.8 ppm; 139.4 ppm; 144.9 ppm; 147.5 ppm; 183.22 ppm. HRMS Calcd. for C₃₃H₂₆N₂S₂O₂ [M + H]: 547.15085, found: 547.15302. The reaction yield was 80%; 0.78 g of red solid was separated (mp. 237–241 °C).

2.2. General Procedure for the Synthesis of Curcumin Derivatives (B1–B7)

The appropriate curcuminoids (50 mg) were dissolved in diethyl ether (2 mL) and acetic anhydride (3 mL) in a round-bottom flask, sealed, and kept under 0 °C for 24 h. Water was added, and the mixture was filtered. The filtered solids were dissolved in acetone and precipitated in water, filtered again, and washed with water.

(1E,6E)-5-(difluoroboryloxy)-1,7-bis(4-hydroxy-3-methoxyphenyl)-1,6-heptadiene-3,5-dione (**B1**). The compound was synthesized using compound **C1**. The reaction yield was 71%; the red solid was separated (mp. 143 °C, lit. 147 °C [22]). ¹H-NMR (*d6*-acetone, 600 MHz), δ = 3.94 ppm (s, 6H), 6.36 ppm (s, 1H), 6.92–6.95 ppm (m, 4H), 7.36 ppm (d, *J* = 8.22 Hz, 2H), 7.48 ppm (s, 2H), 7.95 ppm (d, *J* = 15.54 Hz, 2H); ¹³C-NMR (150 MHz), δ = 56.7 ppm, 100.8 ppm, 112.8 ppm, 114.1 ppm, 122.5 ppm, 133.0 ppm, 146.1 ppm, 150.2 ppm, 154.5 ppm, 161.0 ppm, 181.8 ppm; ¹¹B-NMR (193 MHz), δ = 1.02 ppm; ¹⁹F-NMR (565 MHz), δ = –141.09 ppm. ESI-HRMS Calcd for C₂₁H₁₉BF₂O₆ [M + H]: 417.13155; found: 417.13394.

(1E,6E)-5-(difluoroboryloxy)-1,7-bis(4-methoxyphenyl)-1,6-heptadiene-3,5-dione (**B2**). The compound was synthesized using compound **C2**. The reaction yield was 65%; the orange solid was separated (mp. 175–182 °C, lit. 247–249 °C [23]). ¹H-NMR (*d6*-acetone, 600 MHz), δ = 3.89 ppm (s, 6H), 6.34 ppm (s, 1H), 6.9 ppm (d, *J* = 15.72 Hz, 2H), 6.95 ppm (d, *J* = 15.64 Hz, 2H), 7.06 ppm (d, *J* = 8.8 Hz, 4H), 7.81 ppm (d, *J* = 8.76 Hz, 4H), 7.99 ppm (d, *J* = 15.64 Hz, 1H), 8.04 ppm (d, *J* = 15.76 Hz, 1H); ¹³C-NMR (150 MHz), δ = 55.3 ppm; 55.4 ppm; 101.2 ppm; 111.1 ppm; 111.7 ppm; 118.8 ppm; 124.8 ppm; 127.4 ppm; 146.6 ppm; 149.9 ppm; 153.2 ppm; 179.9 ppm; ¹¹B-NMR (193 MHz), δ = 0.83 ppm; ¹⁹F-NMR (565 MHz), δ = –139.6 ppm. ESI-HRMS Calcd for C₂₁H₁₉BF₂O₄ [M + H]: 384.1339; found: 384.1398.

(1E,6E)-5-(difluoroboryloxy)-1,7-bis(4-chlorophenyl)-1,6-heptadiene-3,5-dione (**B3**). The compound was synthesized using compound **C3**. The reaction yield was 37%; the orange solid was separated (mp. 174–177 °C lit. [24]). ¹H NMR (*d6*-acetone, 600 MHz) δ = 6.37 ppm (s, 1 H), 6.87 ppm (d, *J* = 15.4 Hz, 2 H), 6.94 ppm (d, *J* = 8.2 Hz, 4 H), 7.70 ppm (d, *J* = 8.2 Hz, 4 H), 7.94 ppm (d, *J* = 15.4 Hz, 2 H); ¹³C NMR (150 MHz) δ 101.5 ppm, 116.5 ppm, 118.1 ppm, 126.4 ppm, 132.0 ppm, 146.7 ppm, 161.7 ppm, 180.0 ppm; ¹¹B-NMR (193 MHz), δ = –0.9 ppm, ¹⁹F NMR (565 MHz) δ = –140.2. ESI-HRMS Calcd for C₁₉H₁₂BCl₂F₂O₂ [M–H]: 391.0287; found: 391.0270.

(1E,6E)-5-(difluoroboryloxy)-1,7-bis(4-dimethylaminophenyl)-1,6-heptadiene-3,5-dione (**B4**). The compound was synthesized using 4-dimethylamino-benzaldehyde. The reaction yield

was 8%; the deep red solid was separated (mp. 188 °C, lit. 144 °C [22]). ¹H-NMR (CDCl₃, 600 MHz), δ = 3.13 ppm (s, 12H), 6.21 ppm (s, 1H), 6.68 ppm (d, J = 15.37 Hz, 2H), 6.81 ppm (d, J = 8.96 Hz, 4H), 7.69 ppm (d, J = 8.922 Hz, 4H), 8.02 ppm (d, J = 15.34 Hz, 2H); ¹³C-NMR (150 MHz), δ = 40.13 ppm, 100.4 ppm, 111.9 ppm, 113.1 ppm, 121.6 ppm, 132.1 ppm, 150.1 ppm, 153.3 ppm, 180.7 ppm, 186.9 ppm; ¹¹B-NMR (128 MHz), δ = −0.9 ppm; ¹⁹F-NMR (376 MHz), δ = −140.6 ppm. ESI-HRMS Calcd for C₂₃H₂₅BF₂N₂O₂ [M⁺]: 410.1971; found: 410.1893.

(1E,6E)-5-(difluoroboryloxy)-1,7-bis(4-hydroxyphenyl)-1,6-heptadiene-3,5-dione (**B5**). The compound was synthesized using 4-hydroxy-benzaldehyde. The reaction yield was 37%; the deep blue solid was separated (mp. 165–168 °C, lit. 169 °C [22]). ¹H-NMR (d₆-acetone, 600 MHz), δ = 6.4 ppm (s, 1H), 6.9 ppm (d, J = 15.51 Hz, 2H), 6.97 (d, J = 8.08 Hz, 4H), 7.73 ppm (d, J = 8.136 Hz, 4H), 7.96 ppm (d, J = 15.408 Hz, 2H), 9.73 ppm (s, 2H); ¹³C-NMR (150 MHz), δ = 60 ppm, 101.3 ppm, 116.3 ppm, 117.9 ppm, 126.1 ppm, 131.7 ppm, 146.4 ppm, 161.5 ppm, 179.7 ppm; ¹¹B-NMR (193 MHz), δ = −1.05 ppm; ¹⁹F-NMR (565 MHz), δ = −141.2 ppm. ESI-HRMS Calcd for C₁₉H₁₅BF₂O₄ [M + H] 357.1104; found: 357.1123.

(1E,6E)-5-(difluoroboryloxy)-1,7-bis(3,4-dimethoxyphenyl)-1,6-heptadiene-3,5-dione (**B6**). The compound was synthesized using compound **C6**. The reaction yield was 46%; the bright purple solid was separated (mp. 230–232 °C, lit. 224–226 °C [25]). ¹H-NMR (d₆-acetone, 600 MHz), δ = 3.94 ppm (s, 12H), 6.36 ppm (s, 1H), 6.92–6.96 ppm (m, 4H), 7.36 ppm (d, J = 8.28 Hz, 2H), 7.48 ppm (s, 2H), 7.95 ppm (d, J = 15.56 Hz, 2H); ¹³C-NMR (150 MHz), δ = 55.1 ppm; 56.2 ppm; 102.2 ppm; 111.9 ppm; 112.5 ppm; 119.7 ppm; 125.7 ppm; 128.3 ppm; 147.5 ppm; 150.8 ppm; 154.1 ppm; 180.7 ppm; ¹¹B-NMR (193 MHz), δ = 1.01 ppm; ¹⁹F-NMR (565 MHz), δ = −140.9 ppm. ESI-HRMS Calcd for C₂₃H₂₃BF₂O₆ [M + H]: 445.16285; found: 445.16324.

(1E,6E)-5-(difluoroboryloxy)-1,7-bis(10-methyl-phenothiazinyl)-1,6-heptadiene-3,5-dione (**B7**). The compound was synthesized using compound **C7**. The reaction yield was 83%; the dark purple solid was separated (mp. 175 °C). ¹H-NMR (d₆-acetone, 400 MHz), δ = 3.47 ppm (s, 6H), 6.39 ppm (s, 1H), 6.96–7.04 ppm (m, 6H), 7.16 ppm (d, 2H, J = 7.6 Hz), 7.24 (t, 2H, J = 7.2 Hz, J = 7.8 Hz), 7.62 ppm (s, 2H), 7.67 ppm (d, 2H, J = 8.5 Hz), 7.90 ppm (d, 2H, J = 15.4 Hz); ¹³C-NMR (125 MHz), δ = 35.8 ppm, 102.2 ppm, 115.4 ppm, 117.0 ppm, 118.3 ppm, 119.8 ppm, 123.3 ppm, 125.1 ppm, 125.8 ppm, 127.4 ppm, 128.7 ppm, 129.43 ppm, 129.45 ppm, 129.8 ppm, 131.0 ppm, 132.4 ppm, 144.3 ppm, 145.0 ppm, 162.0 ppm, 180.6 ppm; ¹¹B-NMR (128 MHz), δ = −0.96 ppm; ¹⁹F-NMR (376 MHz), δ = −150.8 ppm. HRMS Calcd. for C₃₃H₂₅BF₂N₂S₂O₂ [M + H]: 595.14913, found: 595.14131.

3. Results

The curcumin derivatives (**C1–C7**) were synthesized by the condensation reaction of the corresponding aldehydes with acetylacetone in the presence of boron trioxide, tri-isopropyl borate, and iso-propylamine in ethyl acetate (Scheme 1). Furthermore, the curcumin derivatives were converted to BF₂ complexes (**B1–B7**) by chelation reaction with BF₃·Et₂O in ethyl acetate and acetic anhydride. The products were purified by precipitation from acetone with water. All compounds were fully characterized by means of NMR spectroscopy (¹H NMR, ¹³C NMR, ¹⁹F NMR, ¹¹B NMR), and HRMS spectroscopy analysis (experimental spectra of **B1–B7** and **C7** are presented in Figures S1–S36). Regarding the proton NMR spectra of the synthesized curcumin derivatives, the peaks of the meta and/or para substituted benzene rings are easily distinguishable in all cases. Each compound contains the trans-olefinic protons of the double bonds present in the carbon atom chain characteristic to AB spin systems, with coupling constants J of 15–16 Hz, which can be observed in every ¹H NMR spectrum. The central methylene group (the meso position) exhibits a singlet peak with a chemical shift in the range of 5.7–6.5 ppm in all cases, which depends on the terminal aromatic moieties and on the nature the substance (curcuminoid or BF₂ complex). The ¹H NMR spectrum of compound **C7** (Figure S35), similarly to compounds **C1–C6**, shows the characteristic peaks of curcuminoids along with the peaks of the phenothiazine moiety in the aromatic region. Since the number of signals in the

proton NMR spectrum are reduced, it can be concluded that the compound is symmetrical (C_s point group symmetry).

The ^1H NMR spectrum of compound **C7** has a tall peak at 5.75 ppm for one proton, suggesting the presence of the enol form. There are also two characteristic doublets in the aromatic region, both with J values of 15.6–16.5 Hz for alkene protons present in the heptadiene spacer, which indicates that all compounds have E configuration. In case of the borondifluoride complexes, the singlet peaks can be observed in the higher region of the aforementioned chemical shift range. In the ^{13}C NMR spectra, at approximately 101 ppm the peak of the enol carbon appears, and for the central methylene carbon in the diketo form a signal can be observed at approximately 56 ppm. In the ^{19}F NMR spectra, sharp singlet peaks were present in all cases, with a chemical shift at approximately -140 ppm. Compound **B7** proved to be an exception, as the singlet signal in the ^{19}F NMR spectrum appeared at -150.8 ppm (Figure S33). The ^{11}B NMR spectrum in each case showed a singlet at approximately -0.9 ppm.

The obtained curcumin- BF_2 complexes incorporate electron-donating moieties at both ends of the conjugated π -system, with an electron-accepting moiety in the middle of the molecule (diketone group), resulting a high absorption maximum between 350–650 nm. As the main difference between the compounds is the terminal aromatic moieties, the absorption maxima can be tuned by altering these aromatic electron donor groups, their electron donating ability being the main influencer of the absorption properties. As can be seen in Figure 2a,b, the presence of strong electron-donating phenothiazinyl moieties results in higher absorption wavelengths, whereas the curcuminoids and BF_2 complexes containing methoxy groups occupy the lower end of the spectrum (Figure 2c,d). In the case of phenothiazinyl derivatives, the influence of BF_2 moiety on the electronic absorption spectra can be seen—the bathochromic shift is significant.

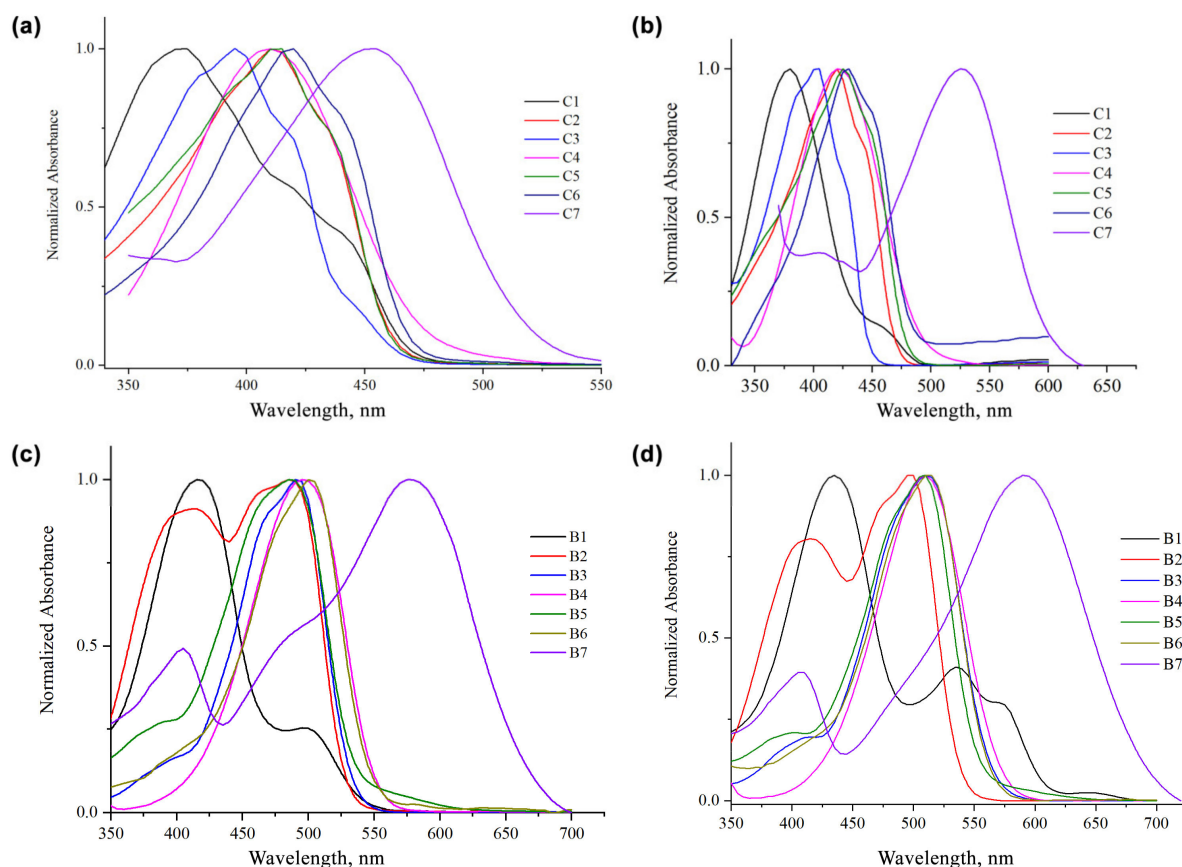


Figure 2. Normalized absorption spectra of compounds **C1–C7** at room temperature in acetone (a) and in DMSO (b); normalized absorption spectra of compounds **B1–B7** in acetone (c) and in DMSO (d) (at $\sim 10^{-5}$ M).

The absorption spectrum is broad and structureless, whereas in n-hexane the spectrum shows some vibration fine structure. The keto-enol equilibrium is favored by non-polar solvents, this can be explained with the stability of the keto form in non-polar solvents, and its contribution may result in blue shifted absorption spectrum. As the solvent polarity increases, the equilibrium is shifted to the enol conformer and the spectral structure is lost. Since curcuminoids are known to exhibit solvatochromism due to their susceptibility to form intermolecular bonds with the solvent molecules [26], the influence of different solvents on the absorption properties of the compounds has been investigated. The absorption band shows a bathochromic shift in more polar solvent, presented in the case of compound **C7** (Figure 3a). The solvent-induced bathochromic shift of the absorption band in case of compound **C7** exhibited a large shift of 36 nm, from 451 nm in low-polar hexane to 487 nm in high-polar DMSO (Figure 3b). The absorption spectrum without normalization of compound **B7** in acetone and DMSO is shown in Figure S37.

The obtained curcumin-BF₂ complexes generally show high absorption coefficients in the range of 400–600 nm (Table 1), most notably in the case of compound **B7**, and also exhibit a bathochromic shift compared their non-complex pairs, as it was expected. The incorporation of the BF₂ moiety into the molecular structure forces it into enol form, increasing the molecular rigidity and stability, thus resulting in higher absorption maxima. Most of the curcumin-BF₂ complexes show a strong fluorescence in the range of 400–650 nm in acetone (Figure 4b).

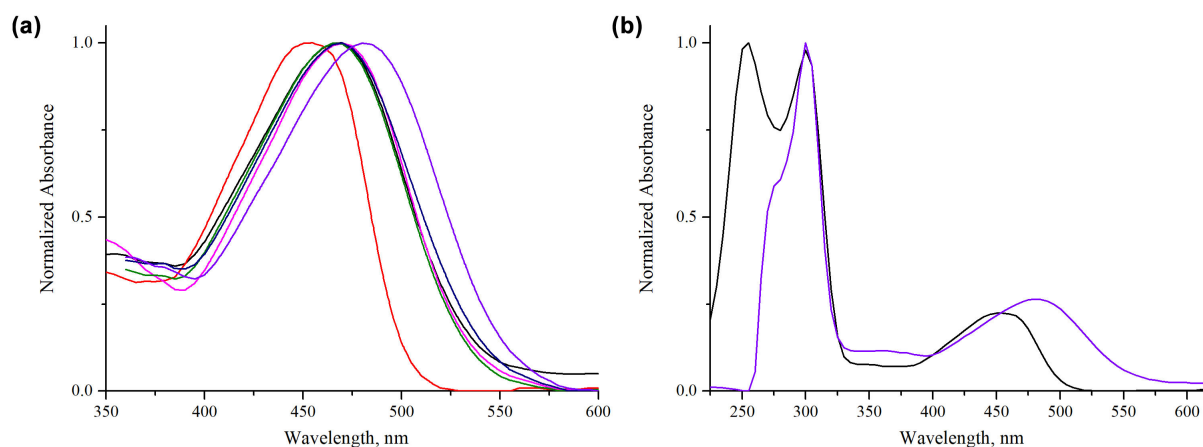


Figure 3. (a) Normalized absorption spectra of compound **C7** in seven different solvents at room temperature: acetone (black), hexane (red), tetrahydrofuran (blue), dichloromethane (pink), acetonitrile (green), ethanol (dark blue), dimethyl sulfoxide (purple); (b) full absorption spectra of compound **C7** in hexane (red) and dimethyl sulfoxide (purple) at room temperature ($\sim 10^{-5}$ M).

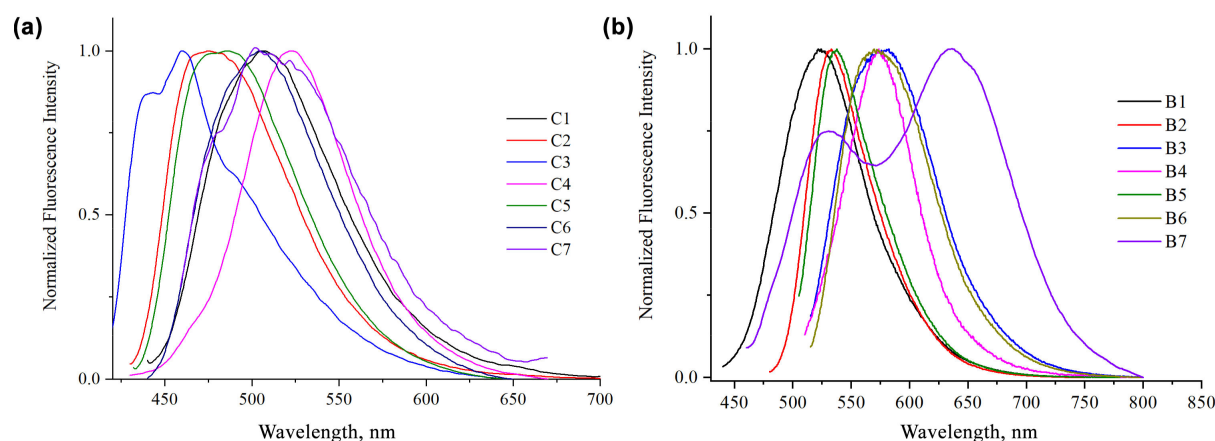


Figure 4. Normalized emission spectra of compounds **C1–C7** (a) and **B1–B7** (b) in acetone at room temperature.

Table 1. Maximum absorption (λ_{abs}) and emission wavelengths (λ_{em}), Stokes shifts, and molar absorption coefficients (ϵ , in $\text{L}\cdot\text{mol}^{-1}\cdot\text{cm}^{-1}$) of compounds **C1–C7**, and **B1–B7** in acetone and DMSO.

Comp.	Acetone				DMSO	
	λ_{abs} (nm)	λ_{em} (nm)	Stokes Shift (cm^{-1})	ϵ	λ_{abs} (nm)	ϵ
C1	374, 422	525	7690	64,900	396, 423	17,689
C2	411	475	3278	52,140	420	26,592
C3	396, 420	461	3561	30,980	403	18,107
C4	409	522	5293	20,730	422	19,281
C5	413	485	3595	48,020	425	35,730
C6	418	504	4082	47,340	430	11,903
C7	350, 468	522	2210	89,712	404, 526	45,035
B1	418, 502	524	4839	69,500	435, 536, 572	134,245
B2	405, 462, 482	532	5894	68,620	414, 498	87,471
B3	500	534	1273	45,324	514	66,212
B4	343, 490	575	3017	47,790	509	67,862
B5	465, 486	538	2918	32,081	510	69,607
B6	474, 498	570	3553	54,810	515	45,778
B7	399, 565	528, 634	9289	123,700	408, 592	150,760

Comparing the emission spectra of the BF_2 -complexes, compound **B7** displays a red shifted fluorescence emission ($\lambda_{\text{em}} = 634 \text{ nm}$) (Figure 4b) associated with a very large Stokes shift (9289 cm^{-1}).

4. Theoretical Study

4.1. Computational Details

Several initial geometries were considered to find the lowest energy conformer. The ground state geometry of each structure was first optimized in the gas phase using the B3LYP density functional and the 6-31G (d,p) basis set. Frequency calculations at the same level of theory were performed to ensure that optimized geometries correspond to a stationary point. Further geometry optimizations were carried out using the 6-311 + G (d,p) basis set, also, to account for the solvent effect the Polarizable Continuum Model (PCM) [27] was employed. In accordance with the experimental part, all structures were optimized in both acetone and DMSO, whereas in case of compound **C7**, computations were also performed in hexane, tetrahydrofuran, dichloromethane, acetonitrile, and ethanol. Time-dependent density functional theory (TDDFT) was used for computing the vertical excitation energies, for each molecule 20 excited states were calculated. All calculations were performed using the Gaussian 09 computational chemistry software package [28]. The Cartesian coordinates of the lowest energy conformers of **C7** and **B7** optimized in gas phase by the B3LYP/6-311 + G (d,p) method are included in the SI (Tables S1 and S2).

4.2. Computational Results

The lowest energy geometries obtained at the B3LYP/6-311 + G (d,p) level of theory in acetone of the studied curcumin derivatives **C2–C7** are shown in Figure 5, whereas the optimized geometry of curcumin **C1** was presented in Figure 1. For each structure, both the keto and the enol tautomer were investigated in gas phase, acetone and DMSO solvents. Several conformers were considered where the aromatic moiety was rotated with respect to the core fragment. It was concluded that in each case the enol tautomer is the lowest energy one, which in case of curcumin **C1** is in agreement with both the crystal structure [29] and with previously published theoretical conformational analysis [30]. These stability differences were also confirmed when the solvent effect was considered.

One should notice that although the experimental spectra confirm that the enolic proton is in a tautomeric equilibrium, still, those geometries correspond to a transition state, characterized by one imaginary frequency. Therefore, the theoretically calculated symmetry of the planar curcumin analogues is C_s , instead of C_{2v} , whereas compounds **C4**

(because of the terminal dimethylamino group) and **C7** have no symmetry. The theoretical results indicate that the aromatic rings of compounds **C1–C6** are coplanar, whereas in the case of **C7**, only the aromatic rings connecting the central core are within the same plane.

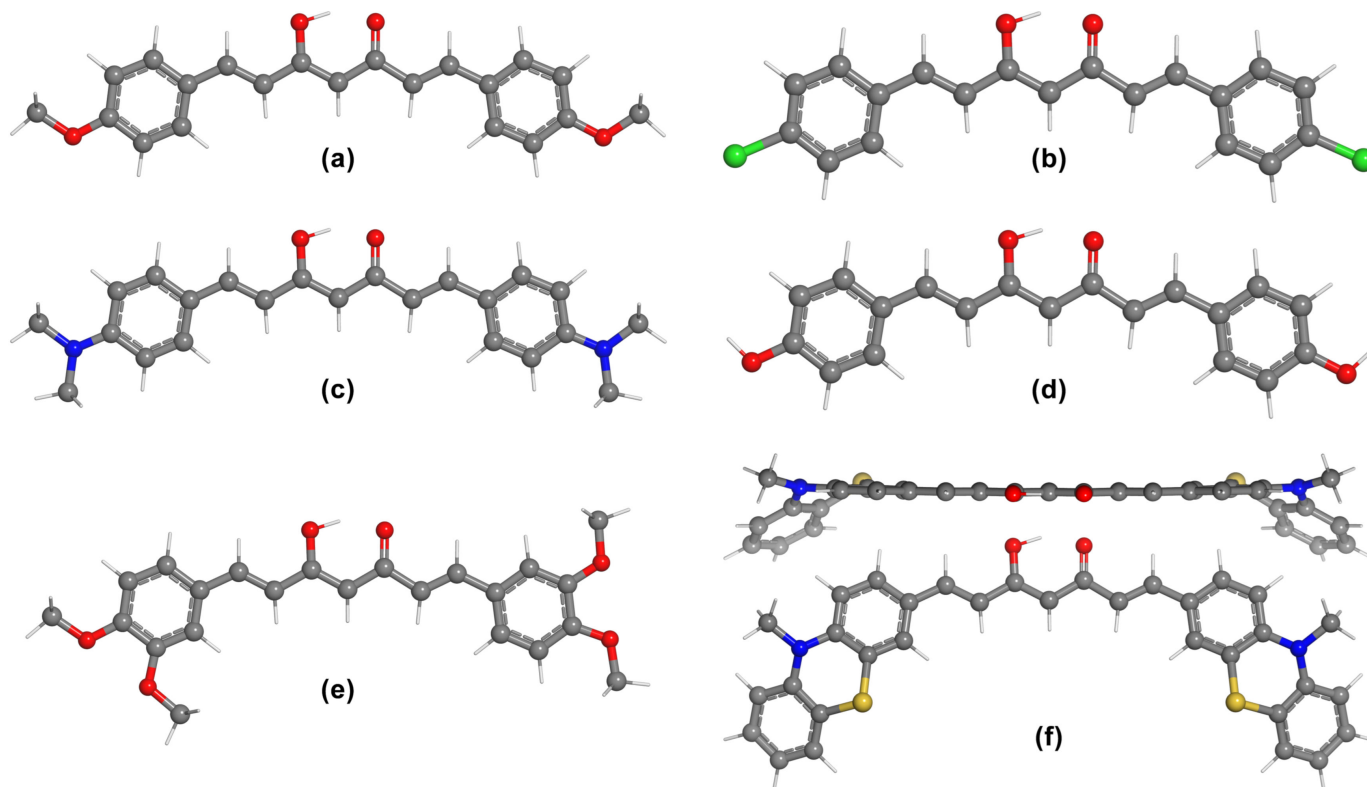


Figure 5. DFT optimized ground state geometries of the enol tautomer of curcumin analogues at the B3LYP/6-311 + G (d,p) level of theory in acetone using the PCM solvation model: (a) **C2–C₅**, (b) **C3–C₅**, (c) **C4–C₁**, (d) **C5–C₅**, (e) **C6–C₅**, (f) **C7–C₁** (top and side view).

In case of the phenothiazine-substituted derivative **C7**, different conformations were considered and optimized at the B3LYP/6-31G (d,p) level of theory. It was found that the lowest energy conformations are the ones where the nitrogen atoms of the phenothiazine groups are oriented in the same direction as the carbonyl groups. Although the structure shown in Figure 5f has the lowest energy, another conformation with relatively identical energy ($\Delta E = 4 \cdot 10^{-4}$ kcal/mol) was also found, with a propeller-like geometry (Figure S38a). It should be noted that the transition state of **C7** has C_5 molecular symmetry, with a relative energy of 1.49 kcal/mol, where the two phenothiazine moieties are identical (Figure S38b), which is in agreement with the experimental observations from the NMR spectra. The conformation where the sulfur and oxygen atoms are on the same side of the molecule (Figure S38c) is higher in energy by 0.52 kcal/mol. The corresponding keto form of **C7** was also investigated (Figure S38d), and it was found to be energetically less stable by 7.53 kcal/mol. For the further geometry optimization of **C7** and calculation of the vertical excitation energies at the 6-311 + G (d,p) level of theory, the effects of seven solvents were considered: acetone, hexane, tetrahydrofuran, dichloromethane, acetonitrile, ethanol, and DMSO.

The optimized geometries obtained at the B3LYP/6-311 + G (d,p) level of theory in acetone of the borondifluoride complexes **B1–B7** are presented in Figure 6. It can be observed, that the ground state geometry of **B1** is different from **C1**, with symmetric orientation of the terminal groups, although the other conformation, shown in Figure S39a is only higher in energy by 0.165 kcal/mol, as computed in gas phase at B3LYP/6-311 + G (d,p). As was already reported [4], the planes defined by the core fragment of the complex and the BF_2 functional group are perpendicular. However, it is an important structural

detail that the structure is only nearly planar, and the BF_2 group is slightly bent on one side of the molecule. As an example, a top view comparison is given in Figure S39b of compounds **C3** and **B3**. This explains why the point group symmetry of molecules **B1–B5** is C_s . The optimized structure of the **B1** complex is in agreement with the geometries computed at B3LYP/6-31G (d), given in [6].

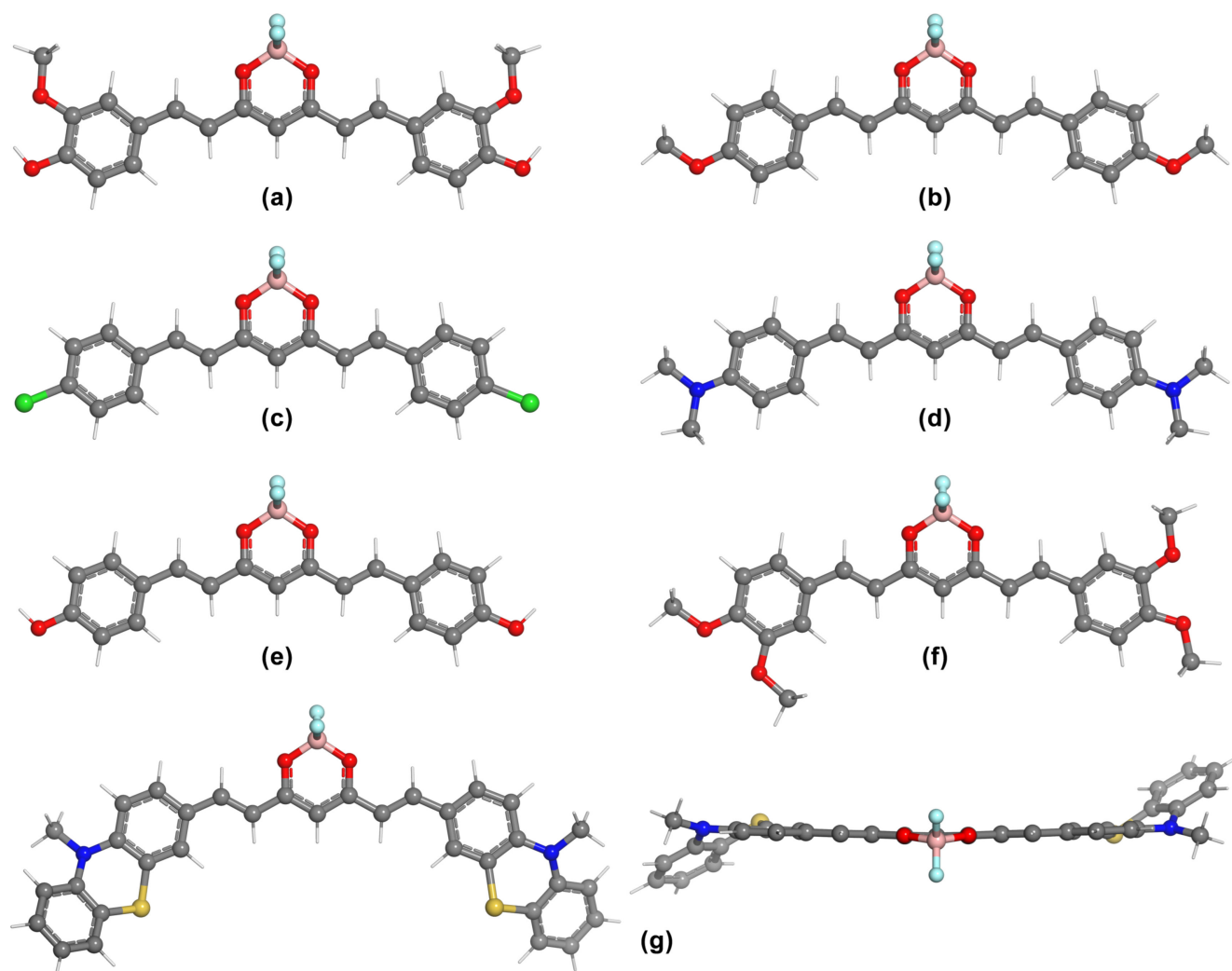


Figure 6. DFT optimized ground state geometries of the borondifluoride complexes at the B3LYP/6-311 + G (d,p) level of theory in acetone using the PCM solvation model: (a) **B1**– C_s , (b) **B2**– C_s , (c) **B3**– C_s , (d) **B4**– C_s , (e) **B5**– C_s , (f) **B6**– C_1 , (g) **B7**– C_1 (side and top view).

In contrast to the observation made in case of the phenothiazine derivative **C7**, the ground state geometry of the novel compound **B7** shown in Figure 6g is lower by $3 \cdot 10^{-3}$ kcal/mol at B3LYP/6-31G (d,p), with respect to the conformer shown in Figure S40a. As it can be observed in Figure S40b, the energy of the molecule increases by $4.6 \cdot 10^{-3}$ kcal/mol in case where the phenothiazine rings are oriented on the opposite side of the structure, compared with the BF_2 moiety. Conformational analysis also demonstrated that similar to **C7**, orientation of both the sulfur and oxygen atoms in the same direction is energetically unfavorable by 0.846 kcal/mol (Figure S40c). Investigation of the transition state of **B7** with C_2 symmetry, where the BF_2 unit is aligned symmetrically with respect to the backbone of the molecule (Figure S40d), is only higher by $2.92 \cdot 10^{-2}$ kcal/mol in energy. The average kinetic energy, which is available at room temperature, would be enough to overcome this energy barrier, and also to enable the conformational interconversion of both **C7** and **B7**.

The theoretically computed absorption wavelengths (λ_{abs} , nm), the vertical excitation energies (E_{ve} , eV), and the corresponding oscillator strengths (f) are reported in Table 2. Using the TD-B3LYP/6-311 + G (d,p) method, the results were obtained for the lowest twenty singlet–singlet transitions of the optimized ground state geometries. In case of each compound, the ground state (S_0) to lowest excited state (S_1) are mainly contributed by the highest occupied molecular orbital (HOMO) to the lowest unoccupied molecular orbital (LUMO) transitions. The oscillator strength was found to be in the range of 1.1–2.3, whereas the HOMO–LUMO transition for these compounds were in the range of 400–650 nm.

Table 2. Theoretical absorption parameters obtained with TD-B3LYP/6-311 + G (d,p) using the PCM solvation model for compounds **C1–C7** (a) and **B1–B7** in different solvents: vertical excitation (λ_{abs} , nm), vertical excitation energy (E_{ve} , eV), and oscillator strength (f).

Solvent	Curcumin Analogs			Difluoroboron-Curcumin Analogs				
		λ_{abs} (nm)	E_{ve} (eV)	f		λ_{abs} (nm)	E_{ve} (eV)	f
Gas phase	C1	426	2.909	1.525	B1	460	2.693	1.618
Acetone		461	2.685	1.677		516	2.399	1.783
DMSO		464	2.668	1.693		521	2.379	1.801
Gas phase	C2	414	2.995	1.741	B2	441	2.808	1.892
Acetone		450	2.758	1.928		495	2.501	2.128
DMSO		453	2.739	1.943		500	2.478	2.146
Gas phase	C3	403	3.074	1.637	B3	425	2.915	1.803
Acetone		426	2.909	1.823		462	2.682	2.018
DMSO		428	2.894	1.837		465	2.663	2.035
Gas phase	C4	455	2.724	1.813	B4	491	2.521	1.986
Acetone		522	2.374	2.051		580	2.134	2.334
DMSO		527	2.350	2.072		588	2.107	2.361
Gas phase	C5	409	3.034	1.610	B5	433	2.858	1.761
Acetone		443	2.802	1.809		485	2.552	2.002
DMSO		446	2.782	1.825		490	2.528	2.021
Gas phase	C6	435	2.850	1.496	B6	471	2.635	1.564
Acetone		471	2.628	1.680		528	2.349	1.807
DMSO		474	2.612	1.698		532	2.330	1.830
Gas phase	C7	495	2.501	1.107	B7	556	2.228	1.130
Acetone		547	2.266	1.314		642	1.930	1.431
DMSO		550	2.252	1.335		648	1.912	1.459
Acetonitrile		548	2.261	1.311				
Dichloromethane		543	2.279	1.329				
Ethanol		547	2.263	1.316				
n-Hexane		520	2.38	1.297				
Tetrahydrofuran		542	2.287	1.321				

The computed absorption wavelengths were found to be shorter by 3–8 nm in acetone than in DMSO, which is in agreement with the experimental results. The computational results indicate, that among the curcumin analogues the novel phenothiazine derivative **C7** has the longest absorption wavelength of 547 and 550 nm in both acetone and DMSO, respectively. This was observed also in case of the corresponding difluoroboron complex **B7**, which has an absorption wavelength at 642 and 648 nm in acetone and DMSO, respectively. The results obtained by the TDDFT investigation of compound **C7** in solvents with different polarity correlates well with the experimental results in Figure 4, the shortest (520 nm) and longest (550 nm) absorption wavelengths were calculated in hexane and DMSO, respectively.

In the case of molecules **C7** and **B7**, the acceptor-donor-acceptor electronic structure of these π -conjugated molecules is highlighted by the plots of the frontier molecular orbitals. It can be observed in Figure 7, that the HOMO orbitals are localized mainly on the terminal

phenothiazine units, which acts as an electron donor group, whereas the LUMO orbitals are located on the electron acceptor core of the molecule, which in case of the BF₂ complex is the dioxaborine ring. The frontier molecular orbital diagrams of compounds **C1–C6** (Figure S41) and **B1–B6** (Figure S42), computed in acetone by B3LYP/6-311 + G (d,p), indicated a similar distribution of the HOMO and LUMO orbitals.

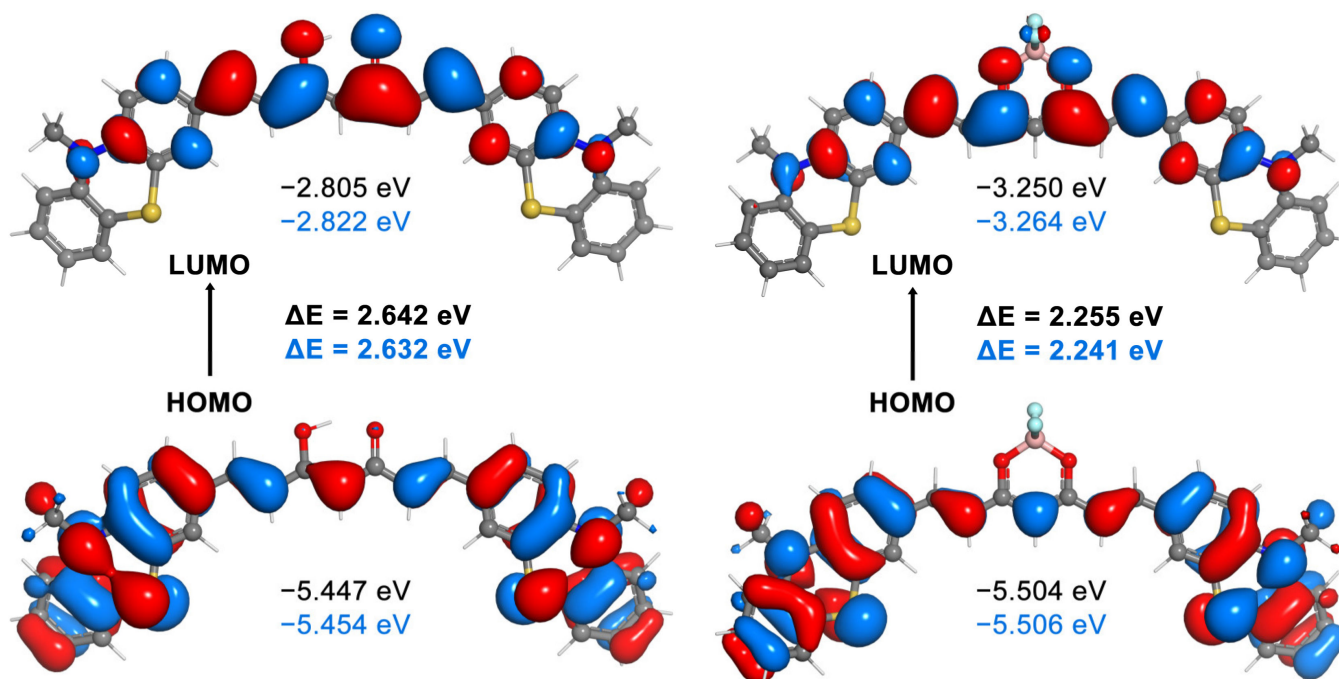


Figure 7. The 0.02 a.u. isosurfaces of the HOMO and LUMO orbitals of compounds **C7** (left) and **B7** (right), and their corresponding energies, computed at the B3LYP/6-311 + G (d,p) level of theory in acetone and DMSO (values in blue) solvents.

In Figure 7, the energy of the frontier molecular orbitals and the energy gap values are indicated for compounds **C7** and **B7**, in both acetone and DMSO, whereas the same data are given for all the other compounds in Figures S41 and S42, evaluated at B3LYP/6-311 + G (d,p). Of all the curcumin analogues, compound **C7** has the smallest energy gap value of 2.64 and 2.63 eV in acetone and DMSO, respectively. Introduction of the BF₂ unit reduces the band gap, which is in agreement with the observed red shift in the case of the difluoroboron complexes. The lowest gap value (2.24 eV) was obtained for the **B7** complex in DMSO solvent. The electron donor character of the functional groups attached to the aromatic units greatly influences the energy gap. Whereas the highest HOMO–LUMO gaps were observed in case of **C3** and **B3** caused by the electron withdrawing chlorine atoms, the electron donor nature of the terminal dimethylamino groups in compounds **C4** and **B4** significantly decreases the energy gap [31]. Correlations between the absorption wavelength computed by TDDFT and HOMO–LUMO gaps are shown in Figure S43.

5. Conclusions

In summary, the synthesis and structural characterization of symmetrical curcumin-analogues **C1–C7** and their corresponding borondifluoride complexes **B1–B7** were reported. Two novel phenothiazine-substituted derivatives, compounds **C7** and **B7**, with enhanced photophysical properties are reported. Upon the incorporation of the BF₂ unit, compound **B7** displays a large red shifted fluorescence emission associated with a very large Stokes shift (9289 cm⁻¹). The ground state geometry of the structures, the electronic properties, and the vertical excitation energies, both in gas phase and in different solvents, were investigated using TDDFT employing the B3LYP functional with 6-311 + G (d,p)

basis set. Whereas curcumin analogs have coplanar aromatic rings, the corresponding BF₂ complexes have only a nearly planar backbone. Although the calculated ground state geometries have lower molecular symmetry compared with those observed in the experimental spectra, interconversion between the conformers and transition state is possible due to the low energy difference. HOMO orbitals are located on the terminal aromatic rings, whereas LUMO is localized on the dioxaborine fragment. The lowest HOMO–LUMO gap values were observed for **C7** and **B7**, caused by the strong electron donor character of the phenothiazine. Future perspectives include fine-tuning the photophysical properties of **B7** by structural modification of the phenothiazine group in different positions, as well as to evaluate the effect of electron acceptor or donor units introduced in the meso position.

Supplementary Materials: The following are available online at <https://www.mdpi.com/article/10.3390/sym13122299/s1>, Figures S1–S37: experimental ¹H NMR, ¹³C NMR, ¹⁹F NMR, ¹¹B NMR, HRMS, and absorption spectra. Figures S38–S40: alternative conformations of **C7** and **B7**. Figures S41 and S42: frontier molecular orbitals diagrams of compounds **C1–C6**, and **B1–B6**, respectively. Figure S43: correlation between computed absorption wavelengths and energy gaps. Tables S1 and S2: optimized cartesian coordinates of **C7** and **B7**.

Author Contributions: Conceptualization and methodology, E.G. and L.C.N.; Experimental investigation, E.G.; Computational study, L.C.N.; Writing—Original Draft Preparation, E.G. and L.C.N.; Writing—Review and Editing, E.G. and L.C.N.; Funding Acquisition, E.G. All authors have read and agreed to the published version of the manuscript.

Funding: This research was funded by the Babeş-Bolyai University, grant number GTC 35278/18 November 2020.

Institutional Review Board Statement: Not applicable.

Informed Consent Statement: Not applicable.

Data Availability Statement: The data that support the findings of this study are available from the corresponding author upon reasonable request.

Conflicts of Interest: The authors declare no conflict of interest.

References

1. Canard, G.; Ponce-Vargas, M.; Jacquemin, D.; Le Guennic, B.; Felouat, A.; Rivoal, M.; Zaborova, E.; D'Aléo, A.; Fages, F. Influence of the electron donor groups on the optical and electrochemical properties of borondifluoride complexes of curcuminoid derivatives: A joint theoretical and experimental study. *RSC Adv.* **2017**, *7*, 10132–10142. [CrossRef]
2. Esatbeyoglu, T.; Huebbe, P.; Ernst, I.M.A.; Chin, D.; Wagner, A.E.; Rimbach, G. Curcumin—from molecule to biological function. *Angew. Chem. Int. Ed.* **2012**, *51*, 5308–5332. [CrossRef]
3. Sui, Z.; Salto, R.; Li, J.; Craik, C.; Ortiz de Montellano, P.R. Inhibition of the HIV-1 and HIV-2 proteases by curcumin and curcumin boron complexes. *Bioorg. Med. Chem.* **1993**, *1*, 415–422. [CrossRef]
4. Bai, G.; Yu, C.; Cheng, C.; Hao, E.; Wei, Y.; Mu, X.; Jiao, L. Syntheses and photophysical properties of BF₂ complexes of curcumin analogues. *Org. Biomol. Chem.* **2014**, *12*, 1618–1626. [CrossRef] [PubMed]
5. Lyu, H.; Wang, D.; Cai, L.; Wang, D.J.; Li, X.M. Synthesis, photophysical and solvatochromic properties of diacetoxyboron complexes with curcumin derivatives. *Spectrochim. Acta A Mol. Biomol. Spectrosc.* **2019**, *220*, 117126. [CrossRef] [PubMed]
6. Margar, S.N.; Rhyman, L.; Ramasami, P.; Sekar, N. Fluorescent difluoroboron-curcumin analogs: An investigation of the electronic structures and photophysical properties. *Spectrochim. Acta A Mol. Biomol. Spectrosc.* **2016**, *152*, 241–251. [CrossRef] [PubMed]
7. Bonardi, L.; Kanaan, H.; Camerel, F.; Jolinat, P.; Retailleau, P.; Ziessel, R. Fine-tuning of yellow or red photo- and electroluminescence of functional difluoro-boradiazaindacene films. *Adv. Funct. Mater.* **2008**, *18*, 401–413. [CrossRef]
8. Chen, P.Z.; Niu, L.Y.; Chen, Y.Z.; Yang, Q.Z. Difluoroboron β-diketone dyes: Spectroscopic properties and applications. *Coord. Chem. Rev.* **2017**, *350*, 196–216. [CrossRef]
9. Kazantzis, K.T.; Koutsonikoli, K.; Mavroidi, B.; Zachariadis, M.; Alexiou, P.; Pelecanou, M.; Politopoulos, K.; Alexandratou, E.; Sagnou, M. Curcumin derivatives as photosensitizers in photodynamic therapy: Photophysical properties and: In vitro studies with prostate cancer cells. *Photochem. Photobiol. Sci.* **2020**, *19*, 193–206. [CrossRef]
10. Ding, L.; Ma, S.; Lou, H.; Sun, L.; Ji, M. Synthesis and biological evaluation of curcumin derivatives with water-soluble groups as potential antitumor agents: An in vitro investigation using tumor cell lines. *Molecules* **2015**, *20*, 21501–21514. [CrossRef]
11. Hua, Y.; Chang, S.; He, J.; Zhang, C.; Zhao, J.; Chen, T.; Wong, W.Y.; Wong, W.K.; Zhu, X. Molecular engineering of simple phenothiazine-based dyes to modulate dye aggregation, charge recombination, and dye regeneration in highly efficient dye-sensitized solar cells. *Chem. Eur. J.* **2014**, *20*, 6300–6308. [CrossRef] [PubMed]

12. Al-Busaidi, I.J.; Haque, A.; Al Rasbi, N.K.; Khan, M.S. Phenothiazine-based derivatives for optoelectronic applications: A review. *Synth. Met.* **2019**, *257*, 116189. [[CrossRef](#)]
13. Luo, J.S.; Wan, Z.Q.; Jia, C.Y. Recent advances in phenothiazine-based dyes for dye-sensitized solar cells. *Chin. Chem. Lett.* **2016**, *27*, 1304–1318. [[CrossRef](#)]
14. Lampe, V.; Milobedzka, J. Studien über Curcumin. *Ber. Dtsch. Chem. Ges.* **1913**, *46*, 2235–2240. [[CrossRef](#)]
15. Pavolini, T.; Gambarin, F.; Grinzato, A.M. Curcumina e curcuminoidi. *Ann. Chim.* **1950**, *40*, 280–291.
16. Pabon, H.J.J. A synthesis of curcumin and related compounds. *Recl. Trav. Chim. Pays-Bas* **1964**, *83*, 379–386. [[CrossRef](#)]
17. Weiss, H.; Reichel, J.; Görls, H.; Schneider, K.R.A.; Micheel, M.; Pröhl, M.; Gottschaldt, M.; Dietzek, B.; Weigand, W. Curcuminoid-BF₂ complexes: Synthesis, fluorescence and optimization of BF₂ group cleavage. *Beilstein J. Org. Chem.* **2017**, *13*, 2264–2272. [[CrossRef](#)] [[PubMed](#)]
18. Venkata Rao, E.; Sudheer, P. Revisiting curcumin chemistry part I: A new strategy for the synthesis of curcuminoids. *Indian J. Pharm. Sci.* **2011**, *73*, 262–270. [[CrossRef](#)]
19. Rao, E.V.; Prasad, Y.R.; Sudheer, P. Revisiting Curcumin Chemistry-Part II: Synthesis of Monomethylcurcumin and Isomeric Demethoxycurcumins and their Characterization. *Indian J. Pharm. Sci.* **2017**, *79*, 820–828. [[CrossRef](#)]
20. Deck, L.M.; Hunsaker, L.A.; Vander Jagt, T.A.; Whalen, L.J.; Royer, R.E.; Vander Jagt, D.L. Activation of anti-oxidant Nrf2 signaling by enone analogues of curcumin. *Eur. J. Med. Chem.* **2018**, *143*, 854–865. [[CrossRef](#)]
21. Weber, W.M.; Hunsaker, L.A.; Abcouwer, S.F.; Deck, L.M.; Vander Jagt, D.L. Anti-oxidant activities of curcumin and related enones. *Bioorg. Med. Chem.* **2005**, *13*, 3811–3820. [[CrossRef](#)] [[PubMed](#)]
22. Sherin, D.R.; Thomas, S.G.; Rajasekharan, K.N. Mechanochemical synthesis of 2,2-difluoro-4, 6-bis(β -styryl)-1,3,2-dioxaborines and their use in cyanide ion sensing. *Heterocycl. Commun.* **2015**, *21*, 381–385. [[CrossRef](#)]
23. Felouat, A.; D'Aléo, A.; Fages, F. Synthesis and photophysical properties of difluoroboron complexes of curcuminoid derivatives bearing different terminal aromatic units and a meso-aryl ring. *J. Org. Chem.* **2013**, *78*, 4446–4455. [[CrossRef](#)] [[PubMed](#)]
24. Liu, K.; Chen, J.; Chojnacki, J.; Zhang, S. BF₃-OEt₂-promoted concise synthesis of difluoroboron-derivatized curcumins from aldehydes and 2,4-pentanedione. *Tetrahedron Lett.* **2013**, *54*, 2070–2073. [[CrossRef](#)]
25. Laali, K.K.; Rathman, B.M.; Bunge, S.D.; Qi, X.; Borosky, G.L. Fluoro-curcuminoids and curcuminoid-BF₂adducts: Synthesis, X-ray structures, bioassay, and computational/docking study. *J. Fluor. Chem.* **2016**, *191*, 29–41. [[CrossRef](#)]
26. Khopde, S.M.; Priyadarsini, K.I.; Palit, D.K.; Mukherjee, T. Effect of solvent on the excited-state photophysical properties of curcumin. *Photochem. Photobiol.* **2000**, *72*, 625–631. [[CrossRef](#)]
27. Tomasi, J.; Mennucci, B.; Cammi, R. Quantum mechanical continuum solvation models. *Chem. Rev.* **2005**, *105*, 2999–3093. [[CrossRef](#)] [[PubMed](#)]
28. Frisch, M.J.; Trucks, G.W.; Schlegel, H.B.; Scuseria, G.E.; Robb, M.A.; Cheeseman, J.R.; Scalmani, G.; Barone, V.; Mennucci, B.; Petersson, G.A.; et al. *Gaussian 09, Revision E.01*; Gaussian, Inc.: Wallingford, CT, USA, 2009.
29. Mary, C.P.V.; Vijayakumar, S.; Shankar, R. Metal chelating ability and antioxidant properties of Curcumin-metal complexes—A DFT approach. *J. Mol. Graph. Modell.* **2018**, *79*, 1–14. [[CrossRef](#)] [[PubMed](#)]
30. Parimita, S.P.; Ramshankar, Y.V.; Suresh, S.; Row, T.N.G. Redetermination of curcumin: (1E,4Z,6E)-5-hydroxy-1,7-bis(4-hydroxy-3-methoxy-phenyl)hepta-1,4,6-trien-3-one. *Acta Crystallogr. Sect. E Struct. Rep. Online* **2007**, *63*, o860–o862. [[CrossRef](#)]
31. Satalkar, V.; Rusmore, T.A.; Phillips, E.; Pan, X.; Benassi, E.; Wu, Q.; Ran, C.; Shao, Y. Computational modeling of curcumin-based fluorescent probe molecules. *Theor. Chem. Acc.* **2019**, *138*, 29. [[CrossRef](#)]